

# **Pharmacokinetics of sufentanil after epidural administration**

Pawel Wiczling

Agnieszka Bienert

Paulina Okuńska

Agnieszka Borsuk-de Moor

Justyna Ber

January 14, 2025

## **Table of contents**

<b>1</b>	<b>Introduction</b>	<b>2</b>
<b>2</b>	<b>Methods</b>	<b>3</b>
<b>3</b>	<b>Raw Data</b>	<b>4</b>
<b>4</b>	<b>Statistical methods</b>	<b>4</b>
4.1	Final model equations . . . . .	5
4.2	Prior predictive check . . . . .	6
<b>5</b>	<b>Results</b>	<b>8</b>
5.1	Final model parameter estimates . . . . .	8
5.2	Posterior predictive check . . . . .	8
5.3	GOF Plots . . . . .	10
5.4	Covariates . . . . .	10
<b>6</b>	<b>Summary</b>	<b>12</b>
<b>7</b>	<b>Appendix</b>	<b>14</b>
<b>References</b>		<b>16</b>
<b>Licenses</b>		<b>16</b>
<b>Original Computing Environment</b>		<b>17</b>

## 1 Introduction

Sufentanil is an analgesic opioid used during anesthesia and for postoperative analgesia. It is one of the most potent opioids. Compared to fentanyl, it exhibits 5-10 times stronger effects after intravenous administration, with a very rapid onset and short duration of action (Maciejewski, 2012). An advantage of sufentanil is better hemodynamic stability for the patient compared to other opioids (Martín-Rodríguez and Bø, 2019). Due to its characteristics, sufentanil is used for anesthesia in pediatric patients, despite the limited number of published clinical studies describing its pharmacokinetics and pharmacodynamics in this population (Lundeberg and Roelofse, 2011).

The pharmacokinetics of sufentanil has predominantly been studied following intravenous administration. However, several reports describe the use of epidurally administered sufentanil in children, including one study that provides individual pharmacokinetic parameter estimates for each patient (Woloszczuk-Gebicka *et al.*, 2014). Our research group was the first to develop a population-based model to characterize the pharmacokinetics of epidurally administered sufentanil in the pediatric population (Borsuk *et al.*, 2017).

In the retrospective study conducted by our team (Borsuk *et al.*, 2017), it was observed that sufentanil absorption from the epidural space follows flip-flop kinetics. This means that the rate of absorption of sufentanil from the epidural space into systemic circulation may be slower than the rate of drug elimination from the patient's body. Consequently, plasma concentrations rise gradually after drug administration and decline more slowly after dosing ends compared to intravenous administration. Additionally, this pattern prevents sudden high plasma concentrations that are associated with an increased risk of adverse effects.

The published analysis was retrospective and based on data from two observational studies with suboptimal sampling schemes for concentration measurements. As a result, the population pharmacokinetic parameters estimated from this analysis may lack precision and be prone to error. An especially critical factor for accurately determining the absorption rate constant is the sampling scheme, which in this case included only one concentration measurement during the absorption phase.

To confirm the value of the absorption rate constant for sufentanil from the epidural space, a study with an experimental design incorporating more frequent sampling during the absorption phase is necessary. Given the lack of scientific reports on population pharmacokinetic studies of epidurally administered sufentanil in adult patients, conducting a study in this population is strongly recommended.

Some literature suggests rapid systemic absorption of sufentanil after epidural administration Taverne, Ionescu and Nuyten (1992), while other authors report low systemic absorption (Menigaux *et al.*, 2001) and lower plasma concentrations compared to intravenous administration during the first hours post-dose (Geller *et al.*, 1993). The discrepancies in available studies highlight the need for a study that can precisely determine the absorption profile of sufentanil from the epidural space.

Additionally, an analysis of covariance will be conducted using demographic and clinical data to identify relationships between patient characteristics and pharmacokinetic parameters. Developing a population model for epidurally administered sufentanil will improve the prediction of plasma concentrations in patients and, consequently, its analgesic efficacy and potential side effects.

This knowledge will enable the optimization of sufentanil dosing for epidural administration and help prevent adverse effects associated with sufentanil use, which are closely tied to plasma concentration levels.

The aim of this study was to describe changes in plasma concentrations of sufentanil after epidural administration in adults using a population pharmacokinetic model. The main focus was to assess the absorption of sufentanil from the epidural space and confirm the occurrence of flip-flop kinetics as suggested in a previous study conducted in the pediatric population (Borsuk *et al.*, 2017). Additionally, the study investigated relationships between body weight, age and sex and the individual parameters describing sufentanil pharmacokinetics.

## 2 Methods

The study will include male and female patients aged 18-70 years undergoing epidural anesthesia for abdominal surgery. Patients classified as ASA physical status 1-3 for perioperative risk will be eligible for inclusion. The estimated sample size is approximately 40 adult patients.

The clinical study was conducted at the Department of Anesthesiology, Intensive Therapy, and Pain Management of the H. Święcicki Clinical Hospital at Poznan University of Medical Sciences.

Patients undergoing anesthesia for surgery will have an epidural catheter placed, through which an initial dose of sufentanil and a local anesthetic from the amide group (e.g., ropivacaine, bupivacaine) will be administered into the epidural space. The dose will be adjusted based on the type of surgery, the patient's age, demographic data (weight, height, BMI), overall health status, and any comorbidities.

Subsequently, a continuous infusion of the medications into the epidural space will be maintained, tailored to the clinical response. The infusion rate will be adjusted to optimize analgesia while minimizing potential adverse hemodynamic effects. Administration will continue during the immediate postoperative period and for the following three days to manage acute postoperative pain effectively.

During the procedure, throughout the postoperative pain management, and after the cessation of drug administration, blood samples will be collected from patients to measure drug concentrations. The blood sampling schedule will be as follows: 5 minutes after the start of drug administration, 30 minutes, 1 hour, 2 hours, 4 hours, 6 hours, and 12 hours after initiation, followed by every 24 hours, just before the infusion ends, and after the infusion ends at 3 minutes, 5 minutes, 20 minutes, 40 minutes, 1 hour, 2 hours, 6 hours, 12 hours, 36 hours, and 72 hours.

Frequent sampling during the initial phase of drug administration and after the infusion ends is crucial for accurately determining the absorption rate and verifying the presence of flip-flop kinetics.

Blood samples of 2 mL will be centrifuged immediately after collection, and the resulting plasma will be stored under appropriate conditions until drug concentration measurements are performed. Drug concentrations were determined using a validated analytical method [Department of Biopharmacy and Pharmacodynamics, Medical University of Gdańsk]

### 3 Raw Data

The raw data is graphically summarized in Figure 1 and Figure 2.

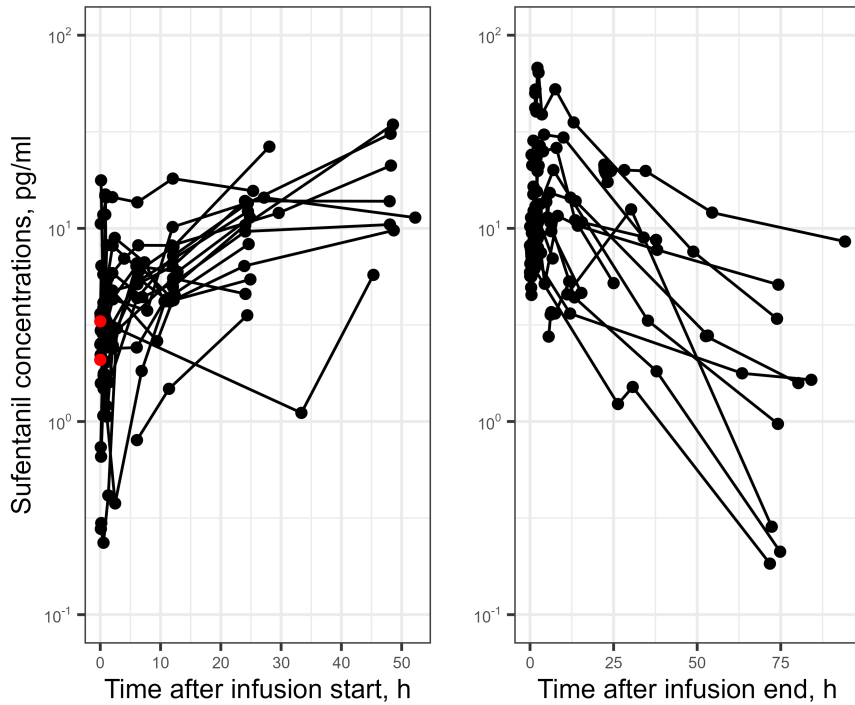


Figure 1: Raw data. Sphagetti plot.

### 4 Statistical methods

Initially, population nonlinear mixed-effect modeling was performed using NONMEM (Version 7.4.0, Icon Development Solutions, Ellicott City, MD, USA) with the gfortran compiler 9.0. NONMEM runs were executed using the bbr package in RStudio. Due to the sparse data, additional literature knowledge on sufentanil disposition was incorporated, and Bayesian methods were employed to enhance the modeling process.

The full Bayesian approach was implemented using Stan/Torsten (<https://metrumresearchgroup.github.io/Torsten/>) programs with the cmdstanr and bbr.bayes packages in RStudio (Carpenter *et al.*, 2017). For the inference, we used four Markov chains with 1000 iterations after 1000 warm up iterations. Convergence diagnostics were performed using Gelman–Rubin statistics and trace plots, and the results indicated that the model results did not diverge. The R code, data, and Stan code used to analyze the data are publicly available in the GitHub repository ([https://github.com/wiczling/sufentanil\\_epidural](https://github.com/wiczling/sufentanil_epidural)).

Following an initial visual inspection of the data, a two-compartment disposition model with first-order absorption was fitted to the concentration-time profiles. However, this model exhibited a significant lack of fit. To address this, the model was modified to allow the disposition parameters

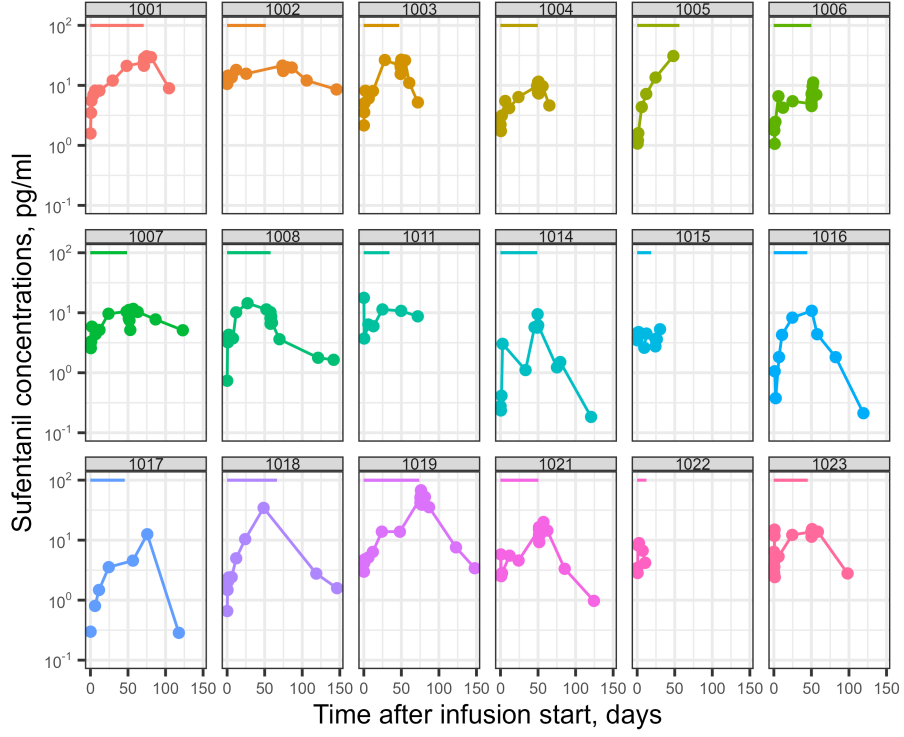


Figure 2: Raw data by ID.

to deviate from the assumed priors. Both models tested suggested that a more complex absorption process was the underlying cause of the misfits. Ultimately, we adopted a two-compartment model with first-order absorption, which provided a satisfactory description of the data.

#### 4.1 Final model equations

The model equitation are as follows:

$$\begin{aligned}
 \frac{dA1}{dt} &= -KA \cdot A1 - KA14 \cdot A1 + KA41 \cdot A4 \\
 \frac{dA4}{dt} &= KA14 \cdot A1 - KA41 \cdot A4 \\
 V_1 \cdot \frac{dC_1}{dt} &= KA \cdot A1 - CL \cdot C_1 - Q \cdot C_1 + Q \cdot C_2 \\
 V_2 \cdot \frac{dC_2}{dt} &= Q \cdot C_1 - Q \cdot C_2
 \end{aligned} \tag{1}$$

where  $A_1$ , and  $A_2$  denote absorption compartments,  $C_1$  and  $C_2$  denote concentration in the central and peripheral compartment. The observed concentrations were modeled assuming proportional error model (additive on a log scale) using a t-distribution to ensure robustness to outliers.

$$\begin{aligned}
 \log C_{Obs_{i,j}} &\sim student\_t(\nu, f(P_i, t_{i,j}), \sigma) \\
 \log P_i &\sim MVN(\log \theta_P, \Omega)
 \end{aligned} \tag{2}$$

where  $P_i = (CL_i, Q_i, V1_i, V2_i, KA_i, KA14_i, KA41_i)$  is a vector of subject-specific parameters,  $f(\cdot)$  corresponds to the above ODE equations,  $MVN$  is a multivariate normal distribution,  $\theta_P$  is a vector of typical values of  $P_i$ . In turn,  $\sigma$  is the scale and  $\Omega$  is the scale matrix for the random effects related to the residual and unexplained between-subject variability. For convenience  $\Omega$  was decomposed to:

$$\Omega = \text{diag}(\omega) \cdot LL' \cdot \text{diag}(\omega) \quad (3)$$

where  $\rho = LL'$  denotes correlation,  $L$  is a lower triangular Cholesky factor for a correlation matrix and  $\omega$  denotes standard deviation for between subject variability.

The Bayesian model requires the specification of priors, which define a plausible range for model parameters based on expectations before observing the data. Priors also establish appropriate scales for the analysis and introduce regularization to enhance model robustness. In this study, weakly informative priors were chosen to align with known facts about sufentanil disposition (Bartkowska-Śniatkowska *et al.*, 2016). The standard deviations for disposition and absorption related parameters were assumed to ensure CV of about 25% and 50%. The weakly informative prior were used to model between-subject variability and residual variability that assumed a %CV of about 40% and 20% with fairly wide uncertainty. Please note that the prior uncertainty is slightly higher than reported in the literature and was used mainly to provide marginal information about model parameters. Consequently, it allowed stabilization of the estimation of model parameters.

$$\begin{aligned} \theta_{CL} &\sim \text{lognormal}(\log(45.3), 0.25), \\ \theta_Q &\sim \text{lognormal}(\log(38.3), 0.25), \\ \theta_{V1} &\sim \text{lognormal}(\log(7.90), 0.25), \\ \theta_{V2} &\sim \text{lognormal}(\log(481), 0.25), \\ \theta_{KA} &\sim \text{lognormal}(\log(1), 0.50), \\ \theta_{KA14} &\sim \text{lognormal}(\log(4.85), 0.50), \\ \theta_{KA41} &\sim \text{lognormal}(\log(0.080), 0.50), \\ \nu &\sim \text{gamma}(2, 0.1), \\ \omega_P &\sim \text{lognormal}(\log(0.4), 0.25), \\ \sigma &\sim \text{lognormal}(\log(0.2), 0.25), \\ LL' &\sim LKJ(10) \end{aligned} \quad (4)$$

LKJ is the Stan default prior for correlation matrices.

## 4.2 Prior predictive check

The prior information was evaluated using prior predictive checks. Prior predictive checking works by simulating new replicated data sets based on the assumed prior information and comparing statistics applied to the replicated data set with the same statistic applied to the original data set. The individual and population prior predictions are shown in Figure 3 and Figure 4. This figures confirm that priors are well shaped and located.

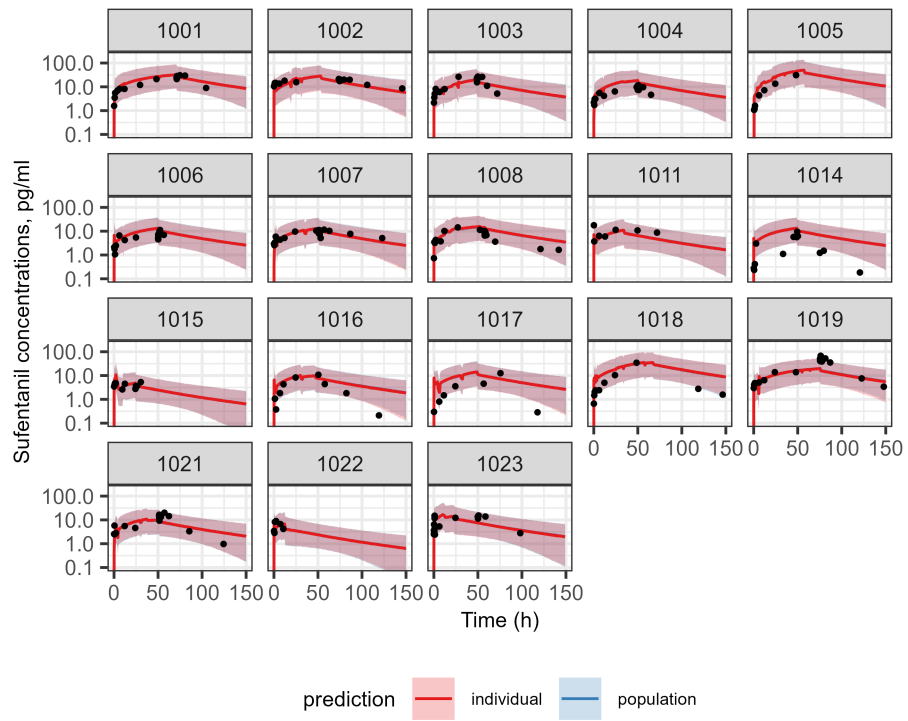


Figure 3: Individual prior predictive check. Plots of observed (symbols), population predicted (blue) and individual predicted (red) concentrations versus time.

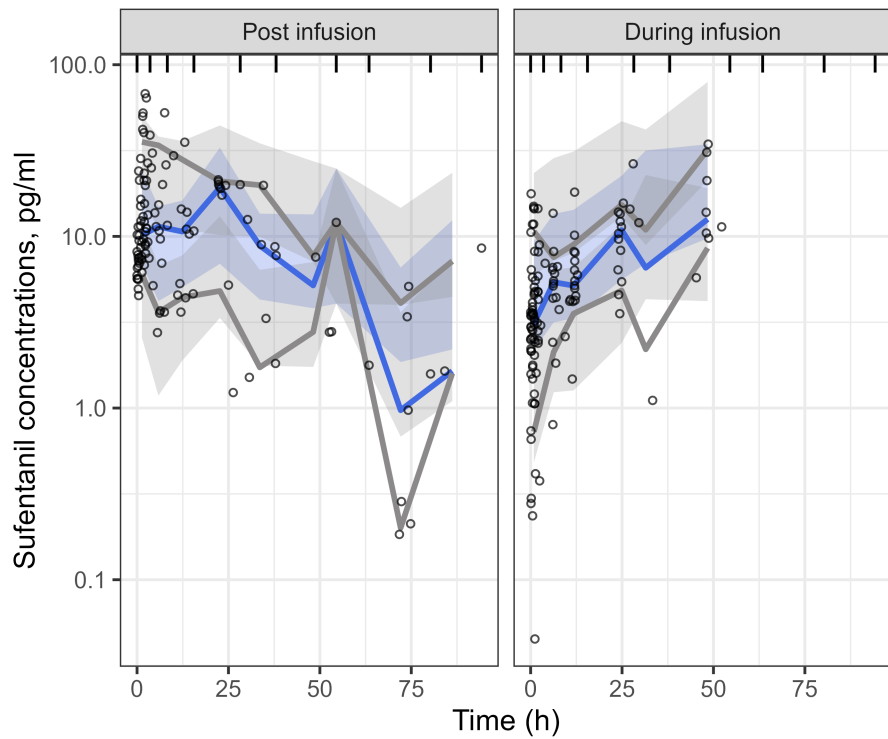


Figure 4: Population prior predictive check.

## 5 Results

### 5.1 Final model parameter estimates

The summary of posterior distribution of model parameters is shown in table 1.

Table 1: Parameter estimates.

parameter	mean	median	sd	90% CI	rhat
lp__	-132	-132	10.7	(-150, -115)	1
CLHat	66.2	65.8	8.34	(53.1, 80.7)	1
QHat	44	43	9.95	(29.7, 61.7)	1
V1Hat	9.35	9.15	2.15	(6.16, 13.2)	1
V2Hat	504	493	117	(337, 719)	1
KAHat	1.99	1.93	0.563	(1.16, 3.02)	1
KA14Hat	10.9	10.5	3.06	(6.62, 16.4)	1
KA41Hat	0.162	0.159	0.0345	(0.111, 0.222)	1.01
omega[1]	0.489	0.483	0.0735	(0.382, 0.617)	1
omega[2]	0.447	0.432	0.124	(0.278, 0.667)	1
omega[3]	1.38	1.38	0.255	(0.951, 1.8)	1.02
omega[4]	0.411	0.397	0.108	(0.261, 0.612)	1
omega[5]	0.378	0.368	0.0897	(0.249, 0.541)	1
omega[6]	0.391	0.381	0.0923	(0.26, 0.559)	1
omega[7]	0.515	0.505	0.115	(0.343, 0.72)	1
sigma	0.31	0.308	0.0261	(0.27, 0.356)	1
nu	3.74	3.51	0.812	(3.04, 5.19)	1

### 5.2 Posterior predictive check

The model performance was assessed by means of Visual Posterior Predictive Checks (VPC). The VPC was calculated based on 1000 datasets simulated based on posterior samples. In this study the 10th, 50th and 90th percentiles were used to summarize the data and VPC prediction. The VPC enables the comparison of the confidence intervals obtained from prediction with the observed data over time. When the corresponding percentile from the observed data falls outside the 95% confidence interval derived from predictions, it is an indication of a model misspecification.

The individual and population predictions are shown in Figure 5. The final model VPC's are shown in Figure 6. The model fittings show that the final PK model accurately described the measured concentrations.

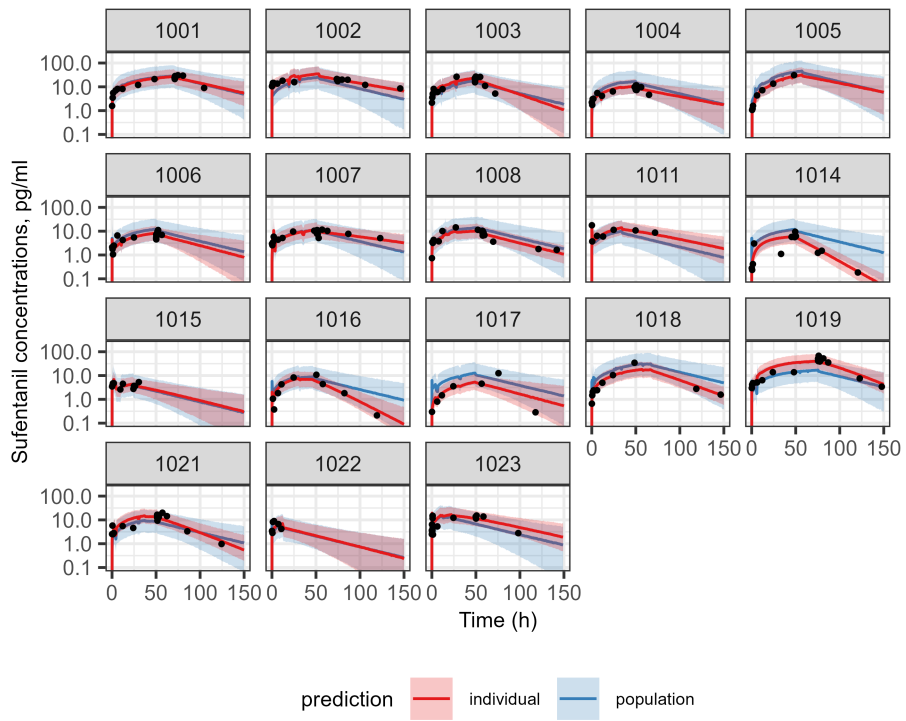


Figure 5: Individual Predictions. Plots of observed (symbols), population predicted (blue) and individual predicted (red) concentrations versus time.

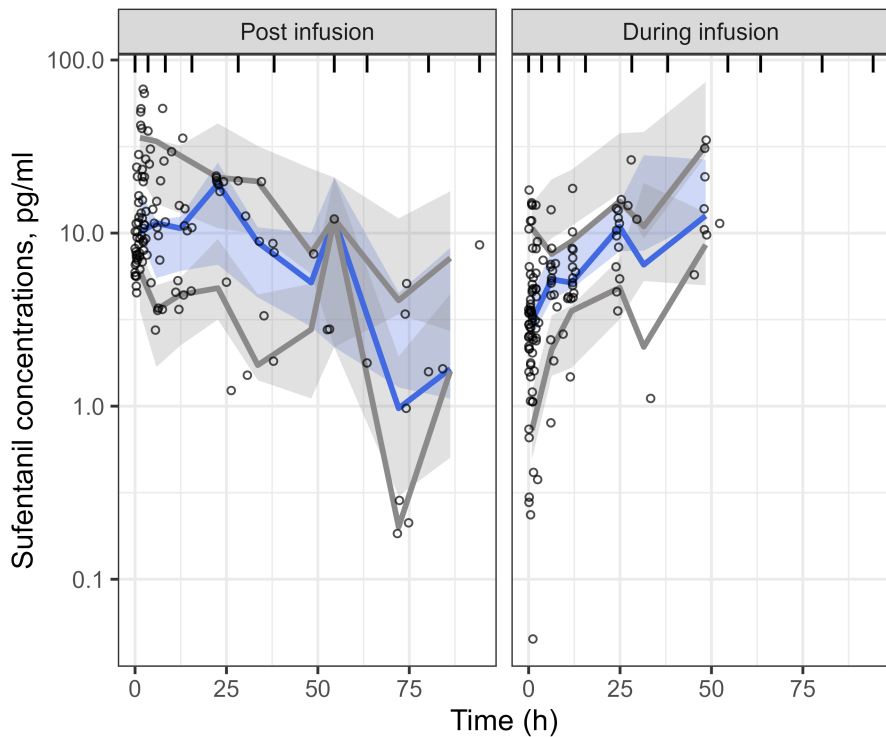


Figure 6: Visual predictive check.

### 5.3 GOF Plots

The individual and population predictions versus observed concentrations are relatively symmetrically distributed around the line of identity indicating good model performance in quantifying the available PK data. The typical goodness-of-fit diagnostic plots for the final model are presented in Figure 7.

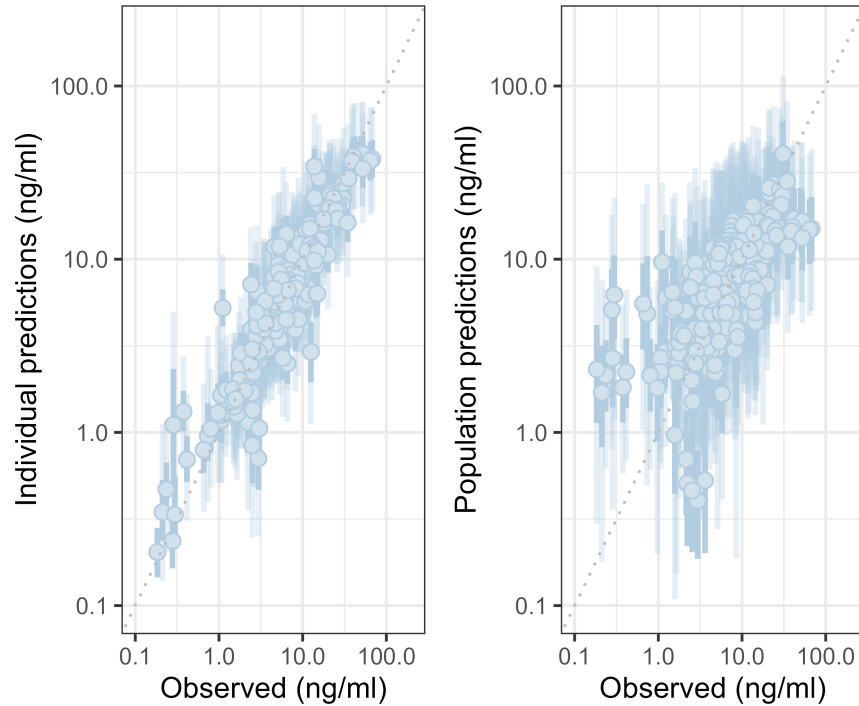


Figure 7: Goodness of fit plots.

### 5.4 Covariates

To evaluate the relationship between individual pharmacokinetic parameters and covariates such as age, body weight, and sex, ETA values were plotted against these variables (Figure 8, Figure 9, Figure 10). This exploratory analysis was limited by the small sample size and substantial uncertainty in individual parameter estimates, leading to high shrinkage.

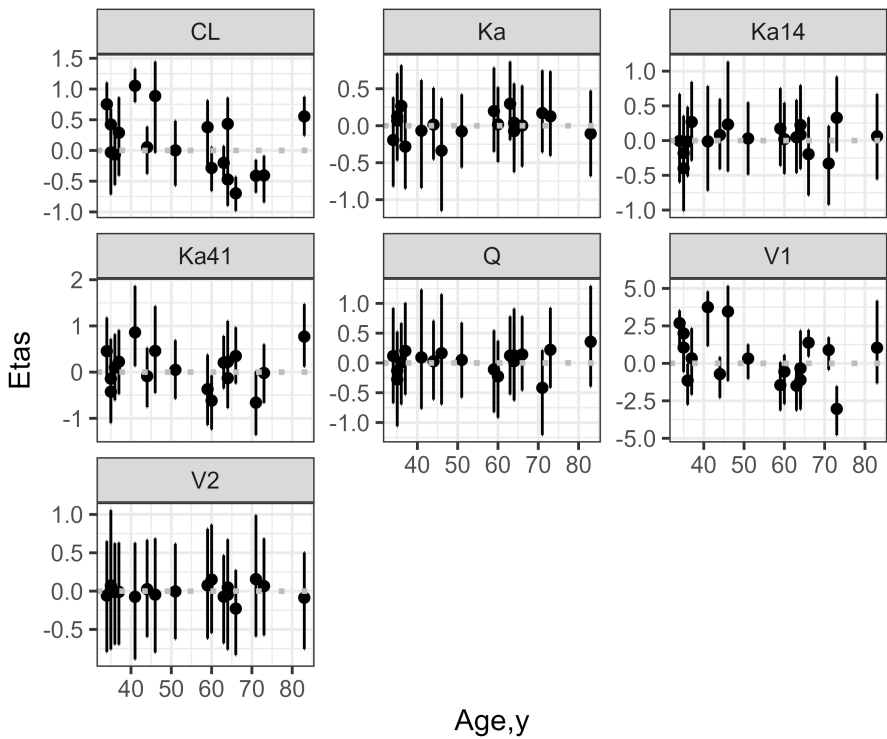


Figure 8: Eta plots for age

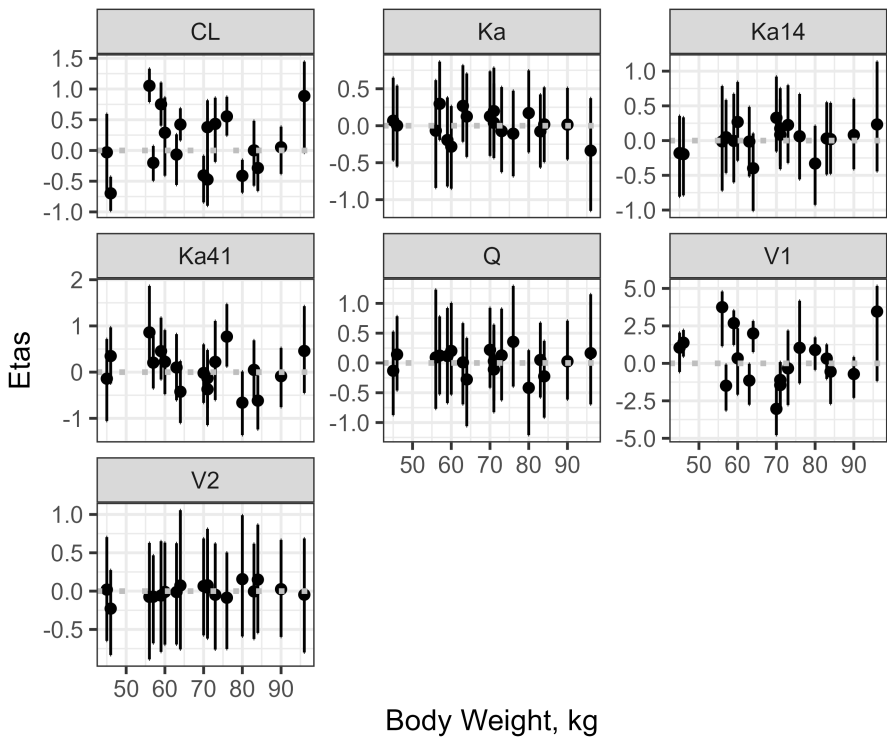


Figure 9: Eta plots for body weight

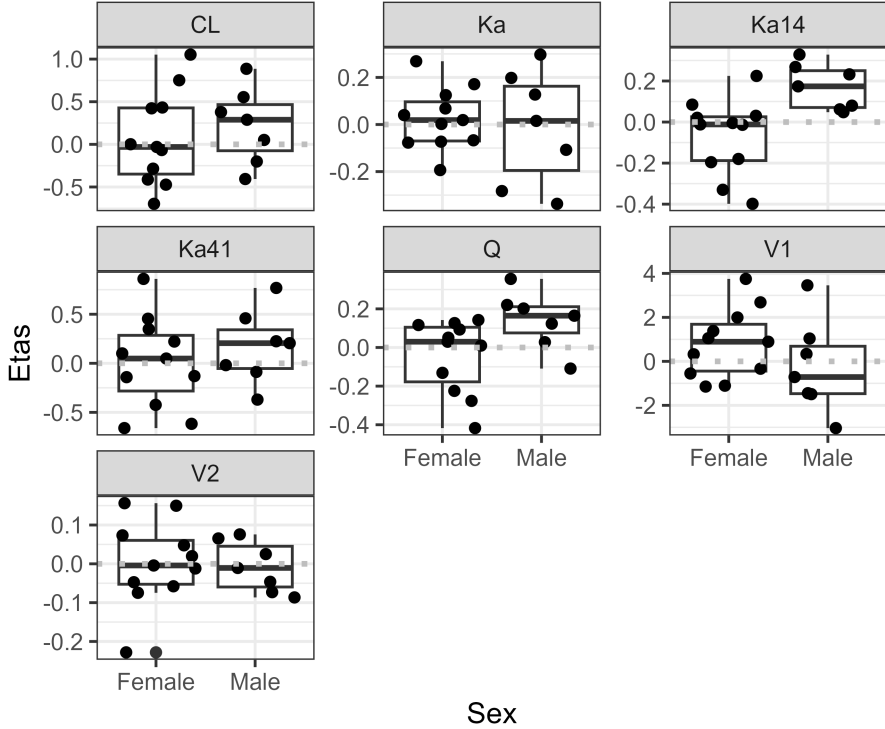


Figure 10: Eta plots for sex

## 6 Summary

What we have learnt?

Figure 11 and Figure 12 summarize the marginal posterior distributions of population-level parameters, between-subject variability (BSV), and residual variability, compared to prior assumptions. The final model pharmacokinetic (PK) parameters align well with existing literature and assumed priors, which is expected given the availability of sufentanil PK data in the literature.

The main finding highlights that the absorption rate constant (to the plasma and to the peripheral compartment) is fast, whereas the redistribution within the epidural space is slow. This suggests that the rate of absorption after the infusion is stopped is primarily governed by the slow redistribution process. Since the half-life of the beta phase of the absorption is about 27 h and of the disposition is much lower 13 h it also suggests the presence of flip-flop kinetics. Thus, the rate of decline of sufentanil in the plasma after epidural administration is controlled by the absorption process.

The systemic absorption of drugs from the epidural space is likely to follow a two-compartment model, as confirmed in a study by (Burm *et al.*, 1987), in which radiolabeled bupivacaine was injected into patients. Burm et al. observed two phases, with the slow phase attributed to the redistribution of the drug from the epidural fat. A similar pattern of absorption can be expected for sufentanil that seems to be well distribute into the epidural fat due its high lipophilicity.

The higher mean posterior clearance compared to prior assumptions (57.3 L/h vs. 46.8 L/h) suggests an increased clearance in the studied population. Other disposition parameters are also higher.

While the estimated values could be influenced by decreased bioavailability, this is unlikely, as it would require sufentanil to be eliminated within the epidural space.

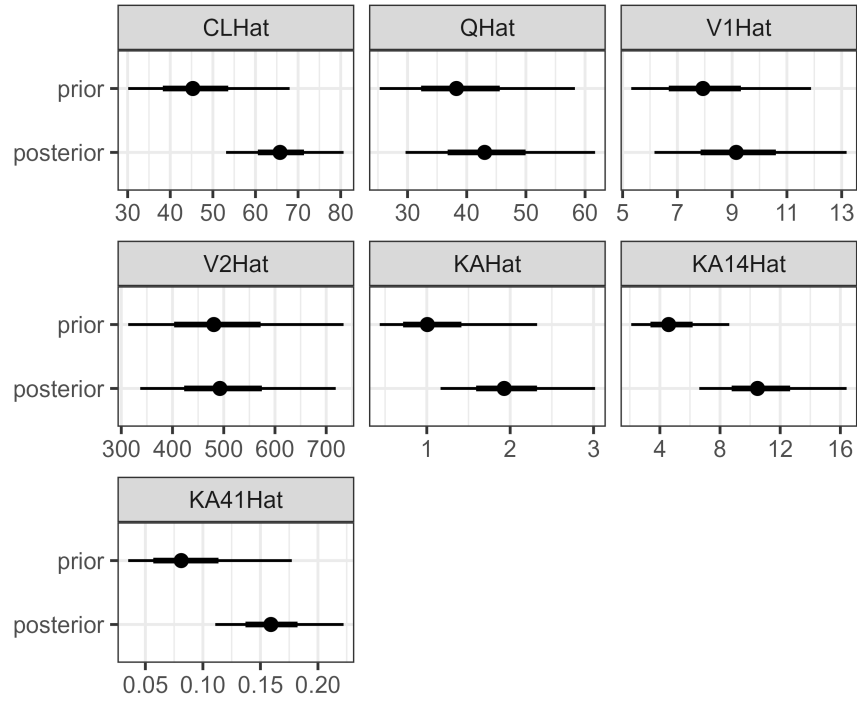


Figure 11: Prior posterior comparisons for population-level parameters.

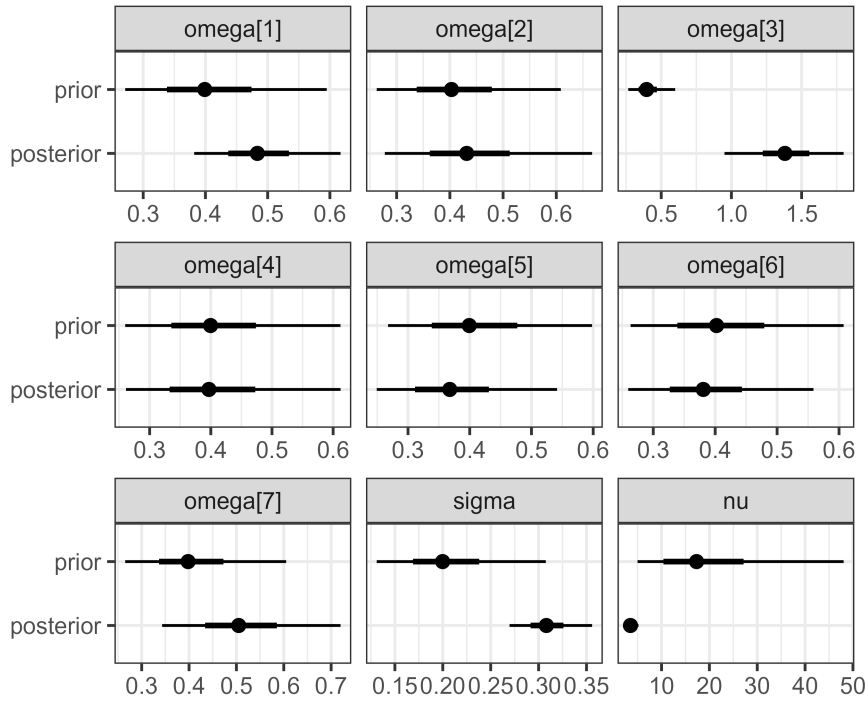


Figure 12: Prior posterior comparisons for random effects

## 7 Appendix

The VPC for the model assuming a first-order classical absorption indicate a substantial lack-of-fit as illustrated in Figure 13 and Figure 14.

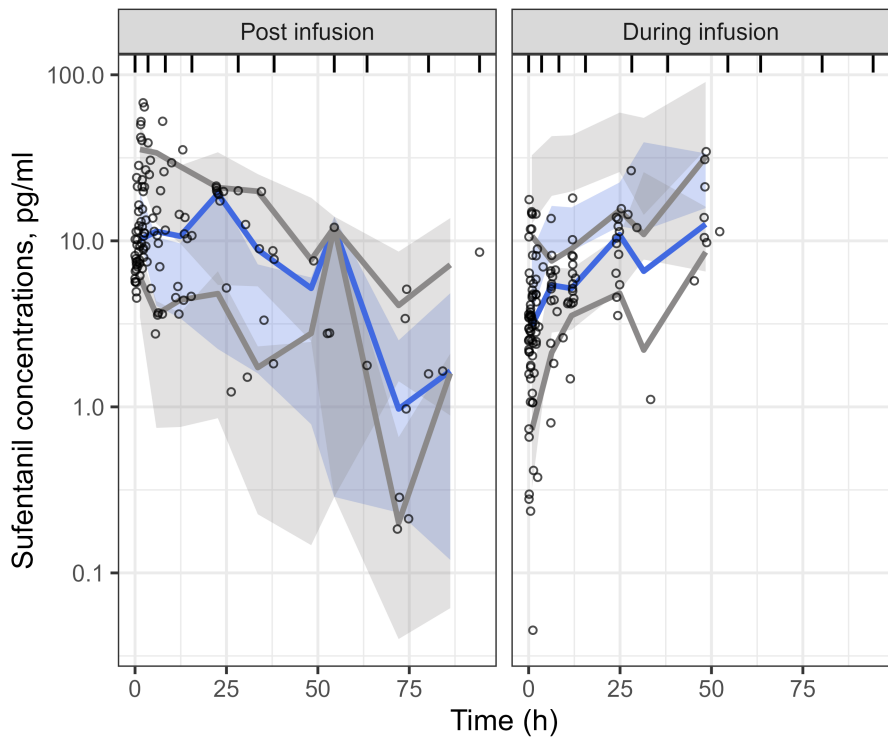


Figure 13: Visual predictive check.

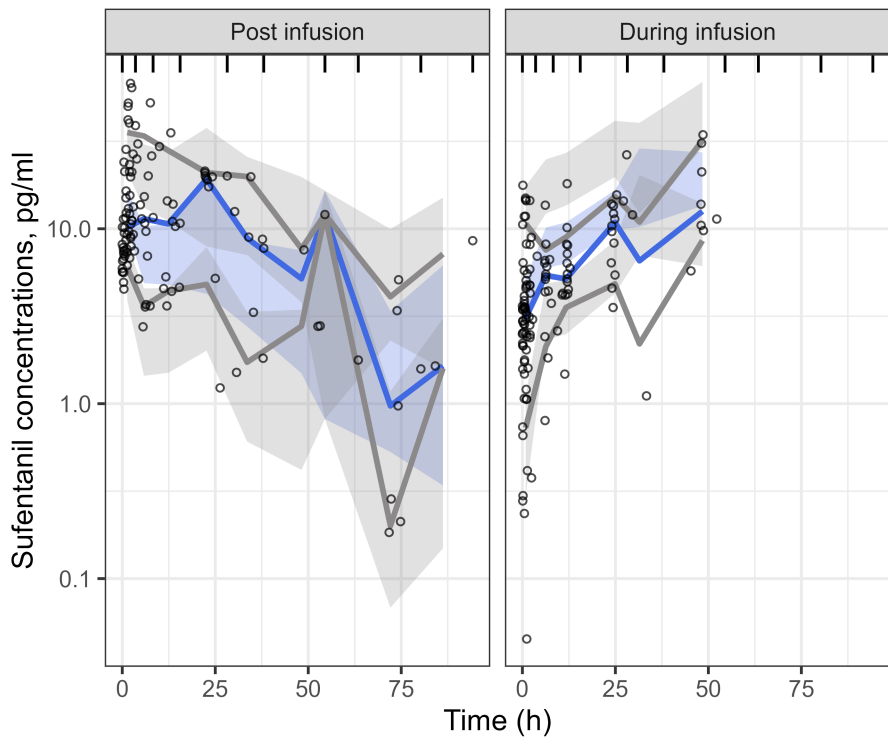


Figure 14: Visual predictive check.

## References

- Bartkowska-Śniatkowska, A., Bienert, A., Wiczling, P., Rosada-Kurasińska, J., Zielińska, M., Warzybok, J., Borsuk, A., Tibboel, D., Kalisz, R. and Grześkowiak, E. (2016) ‘Pharmacokinetics of sufentanil during long-term infusion in critically ill pediatric patients’, *J. Clin. Pharmacol.*, 56(1), pp. 109–115.
- Borsuk, A., Wołoszczuk-Gebicka, B., Bartkowska-Śniatkowska, A., Rosada-Kurasińska, J., Bienert, A. and Wiczling, P. (2017) ‘Flip-flop phenomenon in epidural sufentanil pharmacokinetics: A population study in children and infants’, *JOURNAL OF CLINICAL PHARMACOLOGY*, 57, pp. 1194–1206.
- Burm, A.G.L., Vermeulen, N.P.E., Kleef, J.W. van, Boer, A.G. de, Spierdijk, J. and Breimer, D.D. (1987) ‘Pharmacokinetics of lignocaine and bupivacaine in surgical patients following epidural administration’, *Clin. Pharmacokinet.*, 13(3), pp. 191–203.
- Carpenter, B., Gelman, A., Hoffman, M.D., Lee, D., Goodrich, B., Betancourt, M., Brubaker, M., Guo, J., Li, P. and Riddell, A. (2017) ‘Stan: A probabilistic programming language’, *Journal of statistical software*, 76(1).
- Geller, E., Chrubasik, J., Graf, R., Chrubasik, S. and Schulte-Mönting, J. (1993) ‘A randomized double-blind comparison of epidural sufentanil versus intravenous sufentanil or epidural fentanyl analgesia after major abdominal surgery’, *Anesth. Analg.*, 76(6), pp. 1243–1250.
- Losikoff, P., Fichorova, R., Snyder, B., Rodriguez, I., Cu-Uvin, S., Harwell, J. and Mayer, K.H. (2007) ‘Genital tract interleukin-8 but not interleukin-1beta or interleukin-6 concentration is associated with bacterial vaginosis and its clearance in HIV-infected and HIV-uninfected women’, *Infect. Dis. Obstet. Gynecol.*, 2007, p. 92307.
- Lundeberg, S. and Roelofse, J.A. (2011) ‘Aspects of pharmacokinetics and pharmacodynamics of sufentanil in pediatric practice’, *Paediatr. Anaesth.*, 21(3), pp. 274–279.
- Maciejewski, D. (2012) ‘Sufentanil in anaesthesiology and intensive therapy’, *Anaesthesiol. Intensive Ther.*, 44(1), pp. 35–41.
- Martín-Rodríguez, S. and Bø, K. (2019) ‘Is abdominal hypopressive technique effective in the prevention and treatment of pelvic floor dysfunction? Marketing or evidence from high-quality clinical trials?’, *Br. J. Sports Med.*, 53(2), pp. 135–136.
- Menigaux, C., Guignard, B., Fletcher, D., Sessler, D.I., Levron, J.C. and Chauvin, M. (2001) ‘More epidural than intravenous sufentanil is required to provide comparable postoperative pain relief’, *Anesth. Analg.*, 93(2), pp. 472–6, 4th contents page.
- Taverne, R.H., Ionescu, T.I. and Nuyten, S.T. (1992) ‘Comparative absorption and distribution pharmacokinetics of intravenous and epidural sufentanil for major abdominal surgery’, *Clin. Pharmacokinet.*, 23(3), pp. 231–237.
- Woloszczuk-Gebicka, B., Grabowski, T., Borucka, B. and Karas-Trzeciak, M. (2014) ‘Pharmacokinetics of sufentanil administered with 0.2% ropivacaine as a continuous epidural infusion for postoperative pain relief in infants’, *Paediatr. Anaesth.*, 24(9), pp. 962–967.

## Licenses

- Code & copy; 2025, Paweł Wiczling, licensed under BSD-3.
- Text & copy; 2025, Paweł Wiczling, licensed under CC-BY-NC 4.0.

## Original Computing Environment

```
sessionInfo()

R version 4.3.1 (2023-06-16 ucrt)
Platform: x86_64-w64-mingw32/x64 (64-bit)
Running under: Windows 10 x64 (build 19045)

Matrix products: default

locale:
[1] LC_COLLATE=Polish_Poland.utf8  LC_CTYPE=Polish_Poland.utf8
[3] LC_MONETARY=Polish_Poland.utf8 LC_NUMERIC=C
[5] LC_TIME=Polish_Poland.utf8

time zone: Europe/Warsaw
tzcode source: internal

attached base packages:
[1] stats      graphics   grDevices utils      datasets   methods    base

loaded via a namespace (and not attached):
[1] compiler_4.3.1    fastmap_1.2.0    cli_3.6.3      tools_4.3.1
[5] htmltools_0.5.8.1 rstudioapi_0.16.0  yaml_2.3.10    rmarkdown_2.27
[9] knitr_1.46       jsonlite_1.8.9   xfun_0.50     digest_0.6.37
[13] rlang_1.1.4     evaluate_0.23
```